Snapshot Software Receiver for GNSS in Weak Signal Environments: An Innovative Approach for Galileo E5

Sergio Carrasco-Martos¹, Gustavo López-Risueño¹, David Jiménez-Baños¹, Eberhard Gill², *I European Space Agency, ESA (The Netherlands) 2 Delft University of Technology (The Netherlands)*

BIOGRAPHIES

Sergio Carrasco-Martos has a MSc. in Aerospace Engineering from the Delft University of Technology, a MSc. in Electrical Engineering and Information Technologies from the Universität Stuttgart and a MSc. in Telecommunications Engineering from the Universitat Politècnica de Catalunya. He has held research positions at NASA GSFC and ESA and is currently at the Radionavigation Systems and Techniques section at ESA/ESTEC working on RF navigation sensors for space applications and on GNSS signal processing.

Dr. Gustavo López-Risueño has a PhD (2003) and a MSc. (1998) in Telecommunications Engineering from the Universidad Politécnica de Madrid, Spain. He has held several positions in academia, ESA and NC3A (NATO). Currently, he is a Radionavigation Systems Engineer at ESA/ESTEC working mainly on signal processing for GNSS receivers and monitoring.

David Jiménez-Baños has MSc. degrees in Telecommunications Engineering and Information and Communication Technologies from the Universitat Politècnica de Catalunya. Since 2006 he has been working at the Radio Navigation Systems and Techniques section of ESA/ESTEC, The Netherlands. His main areas of work have been on GNSS signal processing for indoor and AOCS applications in GEO and higher orbits, SBAS systems, and GNSS simulation tools for receiver performance evaluation.

Eberhard Gill, born 1961 in Germany, received a diploma in Physics and holds a PhD in Theoretical Astrophysics of the Eberhard-Karls-University Tuebingen, Germany. He has been working as researcher at the German Aerospace Center (DLR) in the field of precise satellite orbit determination, autonomous navigation and spacecraft formation flying. He has developed a GPS-based onboard navigation system for the BIRD microsatellite. Since 2007, he holds the Chair of Space Systems Engineering of the Delft University of Technology, which developed the nano-satellite Delfi-C3.

ABSTRACT

Global Navigation Satellite System (GNSS) positioning has turned out to be an enabler of Location-Based Services (LBS). This has motivated in recent years an increasing research activity on signal processing techniques for GNSS receivers. However, one main limitation faced by these GNSS receivers is the propagation of GNSS signals in complex scenarios such as urban canyons and indoor, where signals suffer from high attenuation, severe multipath, near-far problem and non-Line Of Sight (LOS) propagation.

These limitations have given rise to highly specialized GNSS receiver architectures, such as snapshot or one shot, overcoming the computational cost of the required processing algorithms and allowing manufacturers the integration of GNSS receivers in mobile platforms. They are commonly known as High Sensitivity GNSS (HS-GNSS) receivers [8].

The European Galileo system will provide additional signals for usage and will most likely improve overall GNSS-based positioning, as well as the role of GNSS technology as an LBS enabler. Research on high-sensitivity Galileo receivers has been quite limited so far; therefore an extensive research activity is necessary. Some effort on E1bc signals has been done, but E5 has not been sufficiently explored [1]. A higher bandwidth and the possibility of using two signals are an advantage in terms of performance in urban canyons or indoor. Nevertheless, a higher bandwidth translates in a higher sampling rate and computational load.

The objective of this work focuses on the design, implementation and performance evaluation of a snapshot software receiver system that exploits the properties of Galileo E5 pilot signals to detect very weak signals, offering a simple yet efficient acquisition-based receiver. The design is based on an acquisition stage that uses efficient signal processing techniques to deliver delay-Doppler estimates and can lead to a position fix without requiring a tracking stage.

INTRODUCTION

Usage of Global Navigation Satellite Systems (GNSS) has become quite common in our society, allowing many applications that are used in our daily lives. From the first satellite navigation system, Transit, developed by the US military in the sixties, to the development of newer systems like Galileo and COMPASS, continuous research on GNSS has led to better accuracies, services and hence applications. This has allowed GNSS to reach the massmarket, one that is currently tending to evolve from hardware-based to software-based systems to reduce their cost and complexity.

With the future deployment of Galileo, GNSS performances will most likely improve and meet future user needs, allowing positioning services in weak signal scenarios (indoor, urban canyons, shaded areas). It is therefore important to consider the strategic potential of Location-Based Services (LBS), where Galileo will quite possibly provide the required accuracy to become an enabler of these services, positioning itself as a privileged candidate to enter a massive business market.

However, Galileo receivers are still in their first phases of matureness, so an extensive research activity needs to follow to enable Galileo receivers to become one day suitable for such applications. Notwithstanding this issue, the flexibility and scalability of Galileo's system architecture allows the accommodation of these needs, and the concept of software receiver discussed here is an example of what the Galileo system will be able to contribute to in the future.

The receiver architecture presented here can be regarded as a HS-GNSS snapshot software receiver architecture. It uses acquisition algorithms that process the pilot components of the Galileo E5 signal in an innovative way. The choice of the E5 signal lies on the fact that through coherent addition of the pilot signals during acquisition, it is possible to achieve a theoretical increase in gain of circa 5 dB with respect to the Galileo E1OS-C band, and about 3 dB with respect to GPS L1 C/A, which is one of the main highlights of the final version of the algorithm. This paper also states the advantages of processing both pilots coherently instead of focusing on an architecture processing just one pilot. Moreover, coherent processing enables to use all the potential of a wideband signal to mitigate multipath

Compared to conventional GNSS receivers that perform coherent correlations with a few code epochs and have acquisition and tracking stages to synchronize the code and carrier phase, HS-GNSS architectures are based on a single-step operation (acquisition) that yields accurate code delay and Doppler shift estimates. They also combine long coherent correlation and non-coherent integration intervals to provide long periods of signal (up to a few seconds), thereby achieving high sensitivities.

In particular, the purpose of the Galileo E5 receiver architecture is to find the visible satellites and obtain code delay and Doppler shift estimates of the impinging LOS signals. Their CNo is estimated as well.

The system takes advantage of the length of the E5 spreading codes (100 ms) to perform coherent correlations between the input signal and the local replica up to this length. A known technique is used that searches for transitions between adjacent secondary codes. A conventional non-coherent integration scheme is used as well.

Moreover, Doppler shift and code delay searches are performed by means of extensive use of the Fast Fourier Transform (FFT) and its properties, delivering reliable results considering the simplicity of the receivers. The FFT also tackles the computational limitations of the algorithm. In addition to this, combination of these coherent correlations with sufficient non-coherent integrations is required to achieve high sensitivities and thus suitable estimates.

Because of all these features, the receiver is able to find the satellites present, overcoming the signal attenuation, multipath reflections and other issues encountered in weak signal scenarios, achieving very high sensitivities for reasonable processing times (around 16 dBHz for 1 second shots). The architecture is hence quite adequate for such applications.

The choice of a snapshot design lies in the simplicity of the receiver in terms of power consumption and processing capacity, as it does not need to work in a continuous mode. Additionally, it works with digitized blocks of data. These facts make it easier to integrate in e.g. handheld devices. The receiver also uses assisted-GNSS data from communication networks to increase its sensitivity and reduce its acquisition time and consequently the Time-To-First-Fix (TTFF) [2].

The paper is structured as follows. First of all, the Galileo E5 pilot signal structure and the signal model used are introduced. Then, the HS-GNSS receiver is presented in detail, pinpointing the advantages of using large coherent correlation intervals and the need of combining them with non-coherent integrations to achieve high sensitivities. Techniques used to mitigate the effects of the Doppler and the code delay in the signal are also explained. To conclude, a performance analysis using data from the European Navigation Laboratory is carried out, showing the improvement of this receiver approach with respect to simpler architectures.

GALILEO E5A / E5B SIGNAL STRUCTURE AND SIGNAL MODEL

The transmitted composite signal E5 is a result of the multiplexing of four components coming from two single

sideband signals, E5a and E5b, with data and pilot channels. Multiplexing is done via an Alternative Binary Offset Carrier AltBOC(15, 10) modulation.

Current Galileo reference spreading codes (or tiered-codes) consist of a secondary code modulating a shorter primary code. The pilot signals of E5a and E5b present each a primary code of 1 ms periodicity, which contains 10230 chips. The secondary sequence has a periodicity of 100 ms and consists of 100 bits of 1 ms duration each. Sub-carrier frequencies f_{E5a} and f_{E5b} are separated a distance of 30.69 MHz, where f_{E5a} is equal to 1176.45 MHz and f_{E5b} is equal to 1207.14 MHz. The central carrier frequency for Galileo E5 is 1191.795 MHz [3].

Thus, a complex envelope model for the E5a and E5b received signals, including data and pilot channels, can be written as (noise free, assuming no additional reflected rays and for one satellite signal only)

$$S_{E5}^{r_{x}}(t) = A_{E5} \sum_{i=a,b} \left\{ \begin{bmatrix} s_{E5i-d}(t - \tau_{E5i}) + j \cdot s_{E5i-p}(t - \tau_{E5i}) \\ e^{j \cdot 2\pi \left[\left(f_{E5i} + f_{E5i-Dop} \right) t - \left(f_{E5i} \cdot \tau_{E5i} \right) + \theta_{E5i} \right]} \right\}$$
(1)

where $s_{E5i-d}(t-\tau_{E5i})$ is the signal (either from E5a or E5b) arriving from the satellite; τ_{E5i} is the delay of the signal affected by the Doppler frequency $f_{E5i-Dop}$, with

$$\tau'_{E5i} = \tau_{E5i} - \frac{f_{E5i-Dop}}{f_{E5i}} \cdot t \tag{2}$$

meaning that the codes will either expand or contract depending on the Doppler shift. The phase term is also affected by this Doppler. A_{E5} is the amplitude of the signal and θ_{E5i} is the received phase.

Moreover, four signal components can be clearly distinguished, two data (d) and two pilot (p) components, where

$$s_{E5i-d}(t - \tau'_{E5i}) = d_{E5i}(t - \tau'_{E5i}) \cdot c_{E5i-d}(t - \tau'_{E5i})$$
 (3)

is either the $E5_{a-d}$ or $E5_{b-d}$ data channel signal component; and

$$s_{E5i-p}(t-\tau'_{E5i}) = c_{E5i-p}(t-\tau'_{E5i})$$
(4)

is either the E5a or E5b pilot channel signal component.

Note that, on the one hand, the data signal carries navigation information, the data symbols of which are not a priori known. On the other hand, the data component $d_{E5i}(t-\tau_{E5i}^{'})$ and the data symbols $c_{E5i-d}(t-\tau_{E5i}^{'})$ are

replaced by a secondary code $c_{E5i-p}(t-\tau_{E5i}')$ in the pilot signal. Since the structure of this secondary code is well known, it is chosen to use the pilot channel for the acquisition algorithm under study, opening an area of research to develop new coherent signal processing techniques thanks to its structure and properties.

Data channels are not considered for processing in this thesis because the message stream (data symbols), are not known, even though their duration is known. This means that a Galileo E5 snapshot receiver willing to process the data channels would rely on less efficient non-coherent correlations. Besides, given that the best possible accuracy is given by the code with largest period, which in the E5 case is the secondary code of the pilots, processing the data channels would not result in better accuracies either.

As a result of the structure of the E5 received signal, a receiver implementation is adopted where the received E5 signal from (1) is processed using two parallel branches. One of these extracts and processes the E5a single sideband pilot signal by means of a correlation with a local code replica of E5a; whereas the other one does the analogous procedure for E5b. The processed signals are added in a coherent way at later acquisition stages, thereby increasing the processing gain of the receiver.

HS-GNSS RECEIVER

Fig. 1 shows the block diagram of the receiver architecture processing E5a and E5b and adding them coherently.

The HS-GNSS receiver computes coherent correlations of 100 ms between the input signal $S_{E5}^{r_x}(t)$ and a delayed and modulated replica of the primary code of the *i*-th satellite: $c_{E5a-p}(t)$ for E5a or $c_{E5b-p}(t)$ for E5b; using digital sample blocks of Galileo E5 data.

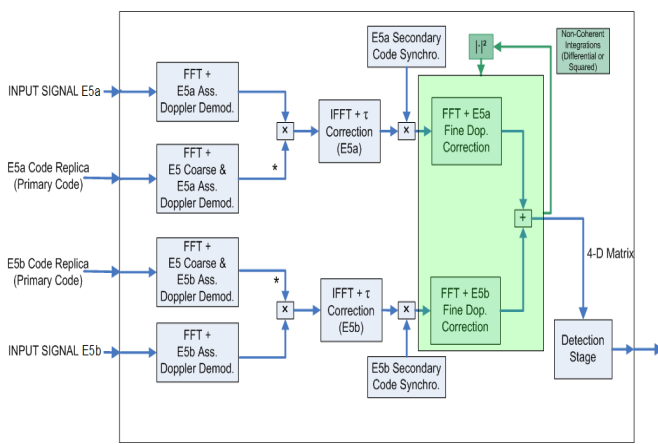


Figure 1 Block diagram of a snapshot receiver performing parallel processing and coherent addition of the pilot signals.

The result of this operation is a 100 ms fine-delay correlation matrix for each signal, $X_{E5a}(\tau_{E5a})$ and $X_{E5b}(\tau_{E5b})$, from which the secondary code is also removed

Although the resulting correlation is 100 ms long, this operation is not performed in a straightforward way. Since the receiver has to find secondary code transitions on the fly, the correlation is calculated through small correlation steps of 1 ms, using the FFT and the overlapsave method.

In total, $(2 \cdot N_s - 1) = 199$ blocks of 1 ms of samples are correlated to ensure a full secondary code sequence falls within, with N_s as the length of the secondary code. Each 1 ms block contains L_c samples. The resulting matrix with dimensions $(2 \cdot N_s - 1) \times L_c$ is the so-called fine-delay correlation matrix, as the correlation peak found in one of the L_c samples of each 1 ms correlation (each of the 199 rows) provides information on the fine code delay.

The origin of the secondary code will be found through a sweeping process that synchronizes a 100 ms replica of the secondary code with 100 blocks of the fine-delay correlation matrix, repeating the process a total of 100 times, thereby obtaining the 100 ms coherent correlations that are mentioned throughout the paper, where one of them will contain a full secondary code sequence.

After adding coherently the contributions from the two synchronized fine-delay correlation matrices and after combining the coherent correlations with non-coherent integrations, a general expression for the delay-Doppler acquisition matrix for any visible satellite can be written as

$$X_{Del-Dop}(\tau_{E5}, f_{E5-Dop}) = \frac{1}{N_{I}} \sum_{r=0}^{N_{I}-1} \begin{bmatrix} r+1 & N_{c}L_{c}T_{c} \\ \sum_{r:N_{c}L_{c}T_{c}} X_{E5a}^{sync} (\tau_{E5a}, f_{E5a-Dop}) + \\ r\cdot N_{c}L_{c}T_{c} \\ + \sum_{r:N_{c}L_{c}T_{c}} X_{E5b}^{sync} (\tau_{E5b}, f_{E5b-Dop}) \end{bmatrix}^{2}$$

$$(5)$$

where $X_{E5a}^{sync} \left(\tau_{E5a}, f_{E5a-Dop} \right)$ and $X_{E5b}^{sync} \left(\tau_{E5b}, f_{E5b-Dop} \right)$ are the delay-Doppler acquisition matrices of E5a and E5b, respectively, after secondary code synchronization (removal). They basically represent the complex correlation between the input signal and the code replica of the current visible satellite. They also contain the fine delay information τ_{E5a} and τ_{E5b} in one axis and the fine Doppler information $f_{E5a-Dop}$ and $f_{E5b-Dop}$ in the other

Additionally, N_I is the number of non-coherent integrations; so $N_c L_c T_c N_I$ becomes the dwell time, where N_c is the number of coherent correlations, L_c stands for the number of chips per primary code and T_c is the primary code period.

HS-GNSS receivers tend to combine a relatively low value of coherent correlations (5, 10 blocks) with large non-coherent integrations (100, 200 blocks), yielding so-called shots (dwell times) of a few seconds. However, for the receiver under discussion it is preferred to use long coherent correlations (100 blocks) to perform an acquisition that takes secondary code transitions into consideration as well.

Furthermore, non-coherent integrations introduce squaring losses that reduce the total processing gain. In addition to this, a short correlation interval would cause problems with secondary code transitions because the beginning of the secondary code is more difficult to locate with just a few milliseconds of signal. If the receiver has to distinguish between the secondary codes of different satellites, the coherent correlation interval must be at least as long as the secondary code period, i.e., greater than or equal to 100 ms, at the same time making it more resistant to near-far.

Fig. 2 shows how a higher sensitivity is achieved for a larger coherent correlation time. It compares sensitivities based on different coherent correlation times. For instance, in order to achieve a sensitivity of 16 dBHz with 20 ms long correlations (which corresponds to the duration of the GPS L1 C/A navigation data bit), 2 seconds of processing time are needed (100 non-coherent integrations).

In comparison, a 2 second shot duration for the 100 ms approach (Galileo E5 tiered code length) would reach a sensitivity of 13.95 dBHz using only 20 non-coherent integrations, showing a gain of 2 dBHz when using 100 ms long coherent correlations. The effects of squaring losses due to an increasing number of non-coherent integrations are hence noticeable.

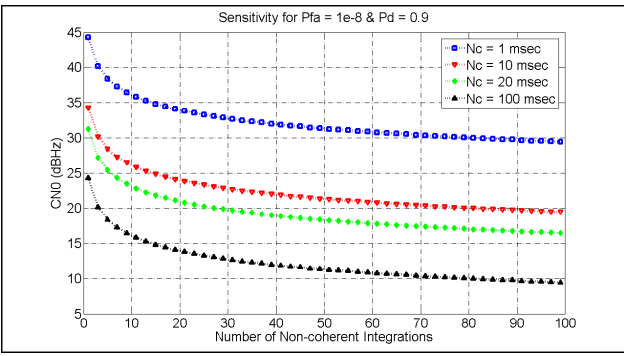


Figure 2 Sensitivity versus non-coherent integrations for several coherent correlation intervals.

Note that the previous discussion is valid for a receiver system with a total energy equal to the coherent sum of the E5 pilots. If the processing is performed such that the signals are added non-coherently (which is also possible), the total energy processed becomes the non-coherent sum of the E5 pilots, smaller than the total energy of the receiver system.

When looking at Fig. 2, this is equivalent as saying that the CN_o must be corrected by adding approximately 1.5 dBHz. Furthermore, if the processing involves only one of the pilots, the CN_o must be corrected by adding 3 dBHz for the same reason, since only half the total energy (one pilot out of two) is processed.

The receiver fills a 4-D matrix with the values from the correlation, where the dimensions are defined as coarse delay, coarse Doppler, fine delay and fine Doppler. First of all, the fine delay and Doppler dimensions are filled for one acquisition matrix. The procedure is repeated 100 times, one for every coarse delay cell search (during the secondary code synchronization process). These operations are repeated for each coarse Doppler bin as well.

The resolutions of the coarse and fine delay and Doppler grid are given by design choices such as coherent correlation time and the signal structure.

The coarse delay resolution is 1 ms due to the length of the primary code, as each one modulates one primary code sequence (1 ms of data or 10230 chips). The coarse delay cell marks the start of a secondary code sequence.

The fine delay resolution is limited by the sample rate, which is therefore chosen such that several samples per chip are selected. It can be improved by linear or quadratic interpolation methods [4].

The use of assisted information reduces the Doppler bin search considerably (to a few KHz). From here, the long coherent correlations allow the receiver architecture to refine the Doppler estimation in two ways. First of all through a coarse estimation that is carried out by means of a bank filter that limits the fine search. Each filter has a bandwidth of 1 KHz. Then, in a later stage a fine Doppler search is done that delivers an accuracy of 5 Hz. This way, just a very small residual remains uncorrected.

The coarse Doppler bandwidth is equal to the inverse of the 1 ms correlation blocks that form each 100 ms coherent correlation, that is, 1 KHz. The resolution is equal to half this value, $\Delta f_{coarse} = 500Hz$.

Fig. 3 illustrates the coarse Doppler as a filter bank of filters of 1 KHz bandwidth separated 500 Hz between each other, such that the overlapping avoids amplitude loss for Doppler frequencies located between two coarse Doppler cells (as seen by comparing the signals at 50 Hz and 450 Hz in the figure).

A well known rule of thumb states that the fine Doppler bin resolution must be roughly equal to

$$\Delta f = \frac{2}{3} \cdot \frac{1}{100ms} \le 6.67 Hz \tag{6}$$

According to common definitions, the fine Doppler bin width of the receiver should be given by the inverse of the dwell time of a set of coherent code correlations. However, this would yield a value of 10 Hz which clearly does not meet the rule. This is solved during a later stage where the length of the fine-delay correlation matrices is doubled by zero-padding their FFT, thus resulting in a fine Doppler resolution of $\Delta f_{fine} = 5Hz$.

A graphical representation of the structure of the 4-D acquisition matrix containing the coarse and fine delay-Doppler estimates can be seen in Fig. 4.

The coherent correlation and filling of the 4-D matrix is subsequently repeated for N_I non-coherent integrations. Then, the 4-D delay-Doppler grid of digital samples is evaluated and the delay and Doppler values maximizing the square cross-correlation are searched for a given space vehicle i,

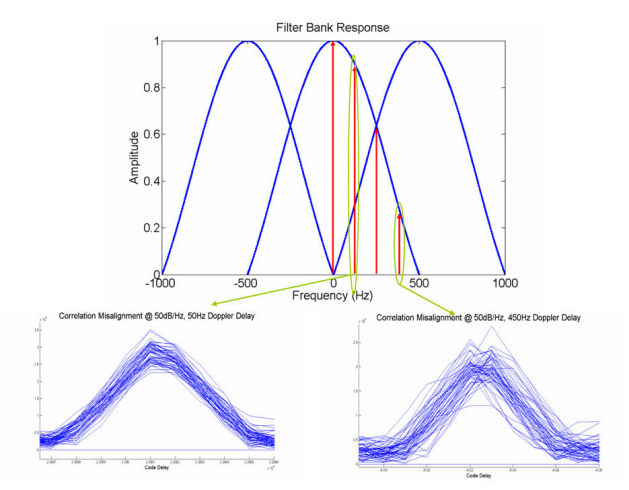


Figure 3 Filter bank response representing the coarse Doppler search cells.

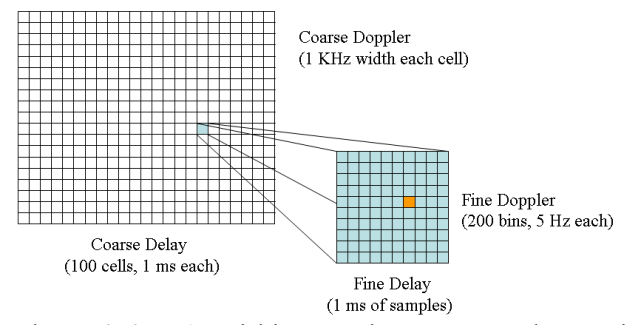


Figure 4 4-D Acquisition matrix structure. The matrix structure is valid for any number N_I of non-coherent integrations.

$$\left\{\hat{\tau}_{E5i}, \hat{f}_{E5-Dop,i}\right\} = \arg\max\left\{X_{Del-Dop,i}\left(\tau_{E5}, f_{E5-Dop}\right)\right\}$$
(7)

A code replica of 199 ms is generated for every coarse delay bin. It is typically simple to compute as one can generate 1 ms of code and replicate it 199 times, meaning that all the blocks are identical. Then, these replicas are correlated with 1 ms blocks of the input signal, using the FFT, yielding the fine-delay correlation matrices (for E5a and E5b).

The treatment of the replica in this case would be that simple if it were not for the presence of the Doppler in the input signal that expands or contracts the spreading codes. If this effect is not taken into account in the replica, a misalignment will occur. To solve this issue, the Doppler has to be included in the code replica. A way to do this is to regard this Doppler effect as a delay and compute it for each 1 ms block [5]. The delay is computed as a function of the current primary code (1 ms block) within the 199 blocks and as a function of the sum of both the coarse and assisted Doppler for the given single sideband signal E5a or E5b.

The idea can be seen in Fig. 5. The figure shows the input signal and the replica synchronized at t = 0ms. It can be seen that at t = 1ms the primary code sequence of the replica starts again. However, due to the Doppler in the input signal, the next primary code sequence of the input signal starts a little bit after t = 1ms. The chips of the input signal have expanded as a consequence of the Doppler effect.

The same issue will appear in successive primary code sequences and a misalignment will eventually occur, which will become clearly noticeable in the correlation matrix, as seen on the top-right corner of the figure. The peaks of the coherent correlation process do not match and drift away, causing degradation in the acquisition.

It can also happen that the discrete form of this delay is a fractional number. This means that the discrete version of the delay can be split in an integer and fractional number of samples. A way to take into account a fractional number of samples consists of an interpolation filter [6].

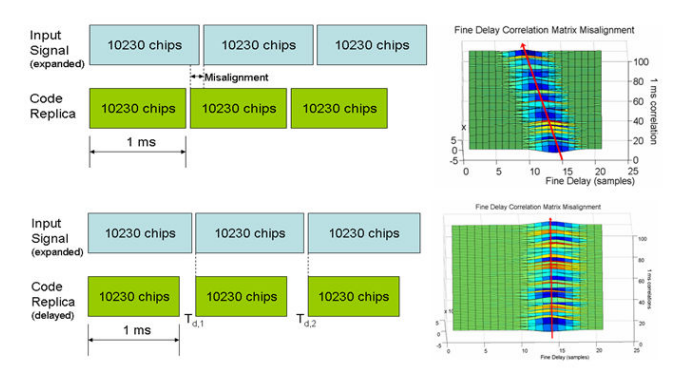


Figure 5 Misalignment between the 1 ms input signal blocks and the code replica blocks before and after inclusion of the Doppler effects in the replica.

In other words, the interpolation filter generates a delay in the code replica such that it resembles the input signal to a degree where the correlation between this replica and the input signal eliminates the misalignment issue. The idea can be appreciated at the bottom of Fig. 5, where each shifted replica block is aligned with its corresponding input signal block.

The advantage of using the delay approximation and the interpolation filter is that the FFT of the code does not need to be recalculated for every 1ms block. The misalignment problem is thereby mitigated and, as a result, two fine-delay correlation matrices are obtained for a given coarse Doppler cell, so only the coarse delay and fine Doppler of the pilots are left to be estimated.

The use of the interpolation filter inside the code replica $c_{E5a-p,replica}(t)$ mitigates, in a coarse way, the effects of the Doppler in the code. So, the frequency dependant term of the time delay expression from $\tau_{E5a}^{'}$ becomes zero (or roughly zero, as a smaller, finer Doppler contribution is still present in the code, but it is not corrected until the detection stage). Reduction of the effects of the Doppler in the code leads therefore to a triangle-shaped correlation $\Delta[t-\tau_{E5a}]$ with a constant delay term, τ_{E5a} .

However, at this point the constant delay term can only give information about the fine delay because the secondary code has not been stripped out of the input signal yet. To that end, a secondary code synchronization step is added, as seen in the block diagram from Fig. 1.

The E5a and E5b fine-delay coherent correlation matrices of dimensions $(2 \cdot N_s - 1) \times L_c$ ensure that a whole secondary code will be contained within them. The secondary code synchronization stage is able to find at which row and column these transitions are located.

For that purpose, a sequence of 100 samples out of the 199 from the coarse delay dimension (rows) of $X_{E5a}(\tau_{E5a})$ is modulated with the 100 bit secondary code sequence, starting from the first millisecond (first row of $X_{E5a}(\tau_{E5a})$). This procedure is repeated along the fine delay dimension of $X_{E5a}(\tau_{E5a})$ a total of L_c times. Each result is stored in a $N_s \times L_c$ matrix.

Then, a second FFT is computed for this matrix. It consists of L_c FFTs computed along each column of N_s samples. The FFT converts the E5a and E5b synchronized coherent correlation matrices in delay-Doppler acquisition matrices that provide information about the fine delay and fine Doppler. It has dimensions $2 \cdot N_s \times L_c$ (the 2 is because zero-padding is used to increase the fine Doppler resolution, as mentioned before).

The $N_s \times L_c$ block of secondary code replicas that modulates a block of the same length from $X_{E5a}(\tau_{E5a})$ can be regarded as a sliding window that perform sweeps along the rows of $X_{E5a}(\tau_{E5a})$. So, after obtaining the first $2 \cdot N_s \times L_c$ delay-Doppler acquisition matrix, the window slides one row down and performs the same operations (synchronization and FFT) from rows 2 to 101 of $X_{E5a}(\tau_{E5a})$. The process is repeated until a total of 100 sweeps are performed.

In the end, there will be 200 delay-Doppler acquisition matrices, 100 for each pilot signal. Two of these matrices will contain an acquisition peak, one per signal (E5a and E5b). The position of the peak will also give information about the coarse delay.

Fig. 6 depicts a case where the signal contains a residual or fine Doppler of 38 Hz modulating the coherent correlation matrix $X_{E5a}(\tau_{E5a})$ (after extraction of the coarse Doppler of 500 Hz resolution through correlation with the replica). The figure shows that one of the L_c columns from $X_{E5a}(\tau_{E5a})$ contains a sequence of 100 samples (100 ms) that coincides with a secondary code sequence. This very same procedure is obviously done for E5b as well.

A $2 \cdot N_s \times 1$ column vector from these matrices will contain the acquisition peaks corresponding to E5a and E5b. However, they will present different relative residual Doppler shifts due to their different sub-carrier frequencies, delivering two acquisition peaks at wrong delay-Doppler cells if this is left uncorrected.

It must also be mentioned that if the matrices are added coherently, the E5a fine-delay correlation matrix will present a term like the following

$$e^{-j\cdot 2\pi \cdot \left(f_{ESa}\cdot \tau_{ESa}\right)} \tag{8}$$

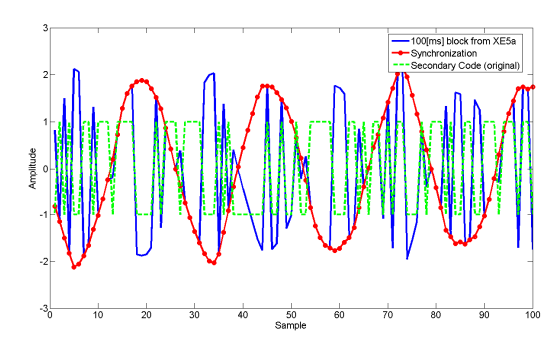


Figure 6 Comparison between the actual secondary code sequence (green) and a 100 ms block of data (blue) with a residual Doppler of 38 Hz containing a whole secondary code sequence. Synchronization is shown in red. Only the real part of the 100 ms block from the fine-delay correlation matrix is shown.

where $f_{E5a}^{'}$ is equal to -15.345 MHz (half the separation of the sub-carrier frequencies from E5a and E5b, with negative sign). E5b will present an analogous term with $f_{E5b}^{'}=15.345MHz$. So, if added coherently, the resulting E5 signal will contain a term that will be equal to zero for certain values of τ_{E5} , namely

$$\tau_{E5} = \frac{1}{6} \cdot (2k - 1) \quad chips \tag{9}$$

with $k = 1, 2, ..., \infty$. This issue is illustrated in Fig. 7. One way to solve this problem consists of cancelling the term in (8) by using one of opposite sign before coherent addition.

Afterwards, detection of the delay-Doppler cell containing the acquisition peak follows. The process detects the peak of every 2D fine-delay correlation matrix for every coarse Doppler and coarse delay cells considered. Then, the maxima are compared with their local threshold, computed based on the local noise floor.

In addition to this, a residual Doppler is adding an error to the correlation results. In a HS-GNSS architecture that uses such long dwell times (1~2 seconds) this problem can lead to synchronization errors. So, after detection has been performed, finer correction methods are applied to the code replica to eliminate the Doppler residual, either by a method of algebraic correction or by a method of fine acquisition [4]. The refined Doppler estimation can also be exploited to improve the code delay resolution beyond the sampling rate. This can be done by either piecewise linear interpolation or quadratic interpolation [4].

Additionally, it is common to estimate the CN_o in snapshot receivers as it is an indicator of the quality of the received signal and can be required for positioning calculations. To that end, a CN_o estimator has been developed based on the methodology from [7]. It is one of a few research efforts that treats this problem in an efficient way for low signal environments.

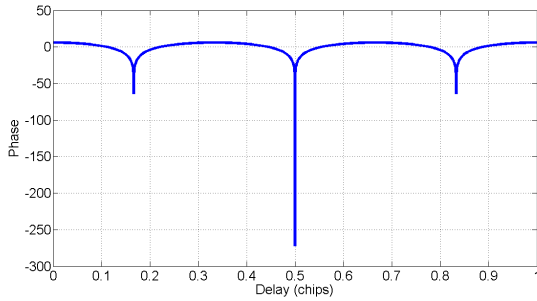


Figure 7 Phase of the coherent sum of both fine-delay correlation matrices causing cancellation of the E5 correlation peak for certain code delay values.

The results section includes experimental results that prove the validity of the estimator in low signal environments.

PERFORMANCE ANALYSIS

Tests were carried out with raw samples from a GNSS BitGrabber equipment connected to the GNSS Spirent signal generator from the European Navigation Laboratory at ESA/ESTEC.

The E5a and E5b signals are extracted from these samples in a conventional way using two different branches and storing them in different files, such that the E5a and E5b sub-carriers can be processed independently at the receiver, only to be added coherently later.

Thus, the input signal of the branch of the receiver that processes the E5a pilot is an E5a baseband, low-pass filtered signal. The analogous is done with the E5b signal for the other branch of the receiver that processes the E5b pilot. This way, at least 95% of signal power is included (the main lobe and several secondary lobes of each pilot).

Low CN_o cases are created in Matlab software by adding digitally-generated noise to the experimental data. This is achieved by adjusting the amplitude of this noise to a specified CN_o and then adding it to the input data.

Other more specific tests are carried out with Matlabgenerated Galileo E5 signals. Low SNR cases have also been created by adding noise.

RECEIVER PERFORMANCE

The performance of the receiver architecture is firstly explained through a graphical example. The sensitivity of the signal in this example is quite large (above 45 dBHz), which would represent a common scenario with high visibility. The Doppler shift is low (184 Hz) so the coarse Doppler search is performed under just one coarse Doppler cell of the filter bank.

The fine delay estimate is given by the fine delay correlation matrix. Thus, E5a and E5b fine-delay correlation matrices for coarse delay cell 46 (which contains the beginning of the secondary code in this case) can be obtained. This matrix is shown in Fig. 8.

The code replica used to compute this correlation is designed according to the techniques explained in the previous section, including a delay and a interpolation filter to take the effects of the Doppler into account.

Afterwards, the fine-delay correlation matrices are modulated by their respective secondary code sequences E5aQ and E5bQ. The shape of the fine-delay correlation vector containing this sequence can be seen in Fig. 9 for E5a.

The shape of the synchronized sequence is a sine function due to the remaining residual or fine Doppler. Thus, the FFT in the direction of the fine delay axis yields a sinc-shaped acquisition peak for the E5a and E5b fine-delay correlation matrices. As the aim is to add the total energy of the pilots, they are added in a coherent way. This is shown in Fig. 10. The result is the delay-Doppler acquisition matrix.

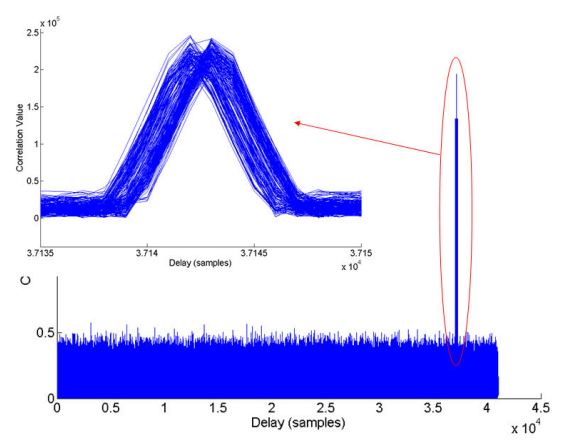


Figure 8 E5a fine-delay correlation matrix for a Spirent signal. The analogous holds for E5b as well.

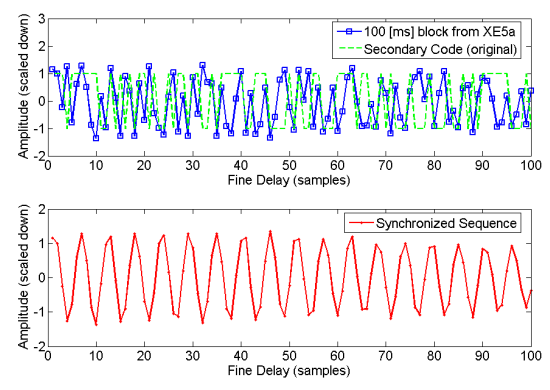


Figure 9 E5a fine-delay correlation matrix from Fig 8 before and after secondary code synchronization. Only the column that contains the secondary code replica is shown.

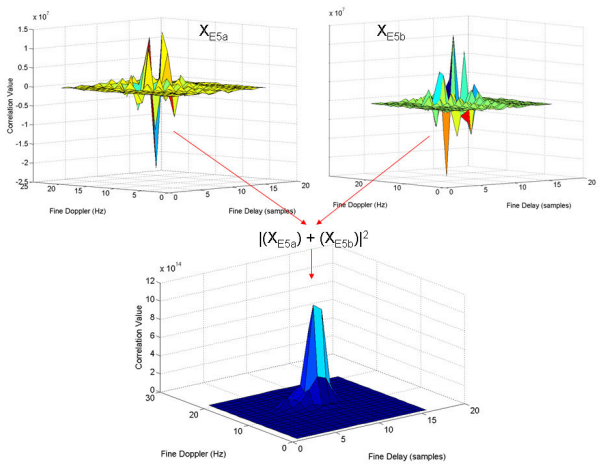


Figure 10 Acquisition peak after coherent addition of the E5a and E5b acquisition matrices. $CN_o = 45 \text{ dBHz}$.

The peak gives information about the fine Doppler and fine delay cell. At the same time, this value belongs to a coarse delay cell that also belongs to a coarse Doppler cell, according to the 4-D matrix structure from Fig. 4.

Fig. 11 and Fig. 12 show a weak signal scenario generated with Spirent where the theoretical limit is circa 13.95 dBHz for $N_I = 20$ non-coherent integrations, therefore the snapshot duration is 2 seconds. Fig. 11 in particular depicts the acquisition peak and threshold for a particular run, where the $\mathrm{CN_o}$ estimator detects a sensitivity value of about 13.84 dBHz.

The receiver performing coherent addition of the pilots is thus able to reach very low sensitivities, according to the theoretical limits shown in Fig. 2.

RESISTANCE TO MULTIPATH

E5 is the GNSS signal with the largest bandwidth (the minimum reference bandwidth needed by the receiver that contains the E5 signal with at least its two main lobes from both sub-carriers is equal to 51.15 MHz).

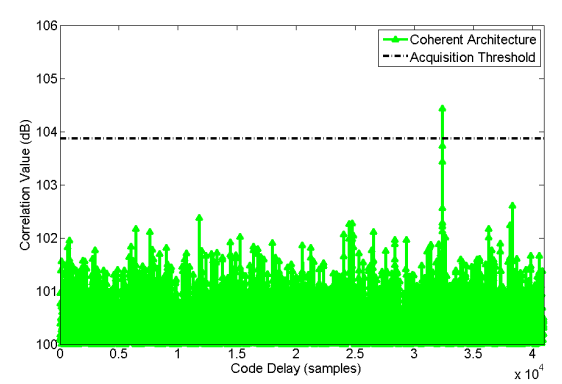


Figure 11 Delay-Doppler acquisition peak above the threshold level. $\text{CN}_{\text{o}} = 13.84 \text{ dBHz}$. 2 seconds of shot duration ($N_I = 20$).

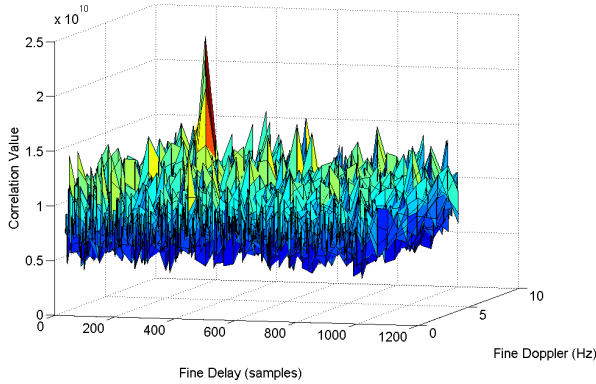


Figure 12 Delay-Doppler acquisition matrix. $CN_o = 13.1$ dBHz. 2 seconds of shot duration ($N_I = 20$).

To compare, Galileo E1OSC has a null-to-null bandwidth of 4 MHz (it uses a Multiplexed-BOC modulation scheme), whereas E5a (and analogously E5b) has a null-to-null bandwidth of 20.46 MHz, hence E5a (or equivalently E5b) has presumably a better resistance to multipath with respect to E1OSC, considering that a larger bandwidth relates to a better resistance to multipath because correlation peaks become narrower for larger bandwidths.

For instance, the E5 architecture discussed here yields narrow correlation peaks that are 195.5 ns. So, peaks coming from multipath reflections will most likely not fall between these 195.5 ns, hence having a smaller impact on acquisition.

An example of this can be seen in Fig. 13 for SV4. With respect to the real, LOS signal, the delay of the multipath signal is equal to 48.88 ns and is attenuated 6 dB. The real signal has a CN_0 of 27 dBHz.

The figure compares the performance of the receiver performing coherent addition of the pilots with a case where the pilots are added non-coherently and the case where only one pilot is processed. The acquisition threshold is also shown and is the same for the three architectures, calculated for the given probability of detection and probability of false alarm, $P_d = 0.9$ and $P_{fa} = 10^{-8}$, respectively, and based on an input signal which total energy is equal to the energy of the coherent sum of the E5 pilots.

According to Fig. 2, the theoretical limit for the coherent architecture for $N_I=1$ is circa 24.5 dBHz. This means this theoretical limit is approximately 26 dBHz and 27.5 dBHz for the non-coherent and 1-pilot architectures, respectively. Nevertheless, the real limits will be larger as it can be seen in Fig. 13, where only the peak from the coherent architecture is detected in this particular run (as it surpasses the threshold).

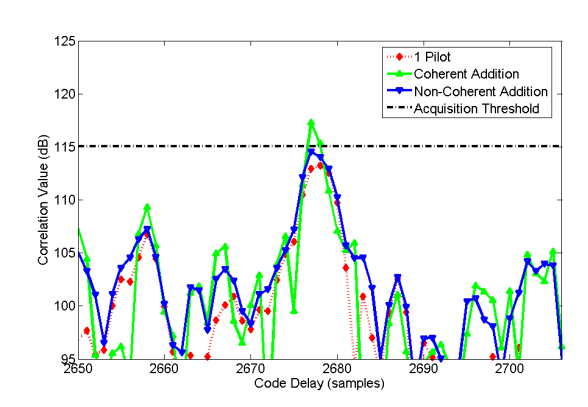


Figure 13 Performance of different receiver architectures against multipath. $N_I = 1$, SV4 and $CN_o = 27$ dBHz for the coherent architecture. See text for discussion.

In this example, only the coherent architecture is able to detect the real peak with high accuracy (6912.011 chips) as the sensitivity is reasonably large for this case, 27 dBHz. The bias is equal to $(10^{-3}/10230) \cdot 3 \times 10^{8} \cdot (6912.011 - 6912) = 0.32m$

Another case is considered where the delay is equal to 24.44 ns. Fig. 14 shows a lower sensitivity case, 21 dBHz, with this delay difference. The peak caused by multipath is attenuated 6 dB and it falls within the real correlation peak.

The coherent and non-coherent architectures are compared again. Both of them are able to detect the right peak. This time, the bias is $(10^{-3}/10230) \cdot 3 \times 10^{8} \cdot (4960.825 - 4961) = 5.13m$.

The resistance to multipath for the architecture processing coherently two pilots is thereby verified.

RESISTANCE TO THE NEAR-FAR PROBLEM

A longer coherent correlation interval together with the addition of two pilots increases the resistance to the near-far problem in the receiver architecture.

To prove that, an example is shown that compares the performance of the coherent architecture with that of a non-coherent architecture, similar to what was done in the previous section about the multipath discussion.

The second case, shown in Fig. 15, represents a weaker signal scenario, where SV14 has a strength of about 19.5 dBHz. It is highly affected by SV16, which has a CN_o of 35 dBHz. Five non-coherent integrations are used, which allow the coherent receiver to reach a theoretical limit of 18.4 dBHz (plus 1.5 dBHz for the non-coherent architecture).

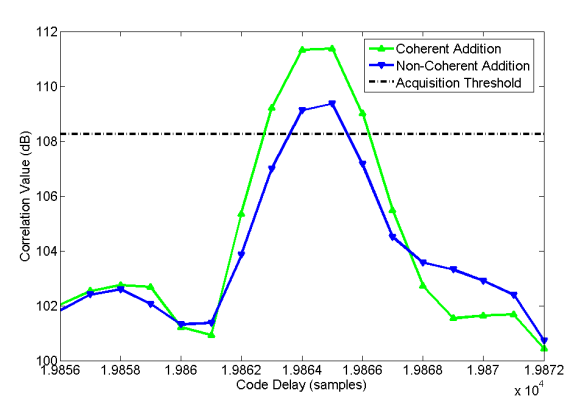


Figure 14 Performance of different receiver configurations against multipath. $N_I = 10$, SV22 and $\mathrm{CN_o} = 21~\mathrm{dBHz}$ for the coherent architecture. See text for discussion.

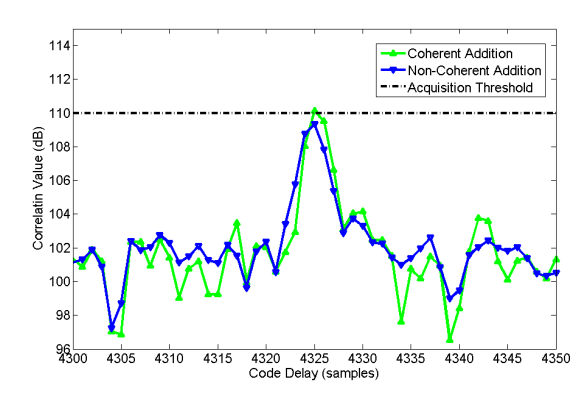


Figure 15 Performance of different receiver configurations against the near-far problem. $N_I=5$, SV14 and $\mathrm{CN_o}=19.5$ dBHz. The stronger signal is due to SV16 and has $\mathrm{CN_o}=35$ dBHz. See text for discussion.

Thus, only the coherent architecture can properly detect the acquisition peak as the other one is below the threshold. The coherent architecture estimates a delay of 1079.983 chips, therefore a bias of $\left(10^{-3}/10230\right)\cdot 3\times 10^{8}\cdot \left(1080-1079.983\right)=0.49m$. The Doppler is estimated accurately to a level of 30 Hz with an uncertainty of less than 5 Hz.

CNo ESTIMATOR PERFORMANCE

The performance of the CN_o estimator is shown in Fig. 16 and Fig. 17. The former shows the CN_o estimator performance for 100 coherent correlations and 10 non-coherent integrations, hence 1 second shots, with $P_{fa} = 10^{-8}$.

According to Fig. 18, which shows the probability of acquisition versus the sensitivity, for a chosen probability of acquisition $P_d = 0.9$, the theoretical limit is equal to 16.1 dBHz. For such a small probability of false alarm, it can be said that the estimator is good.

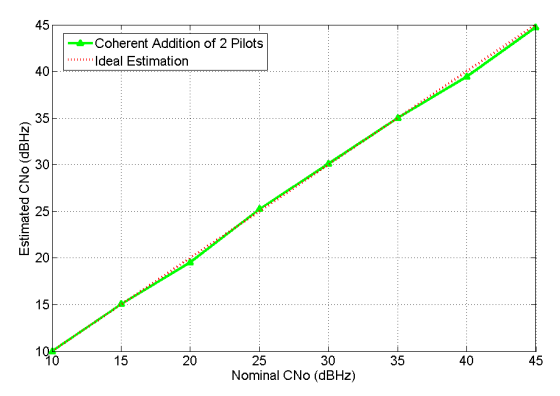


Figure 16 Performance of the CN_o estimator for the architecture performing coherent addition of the pilots. $N_c=100$, $N_I=10$, $P_{fa}=10^{-8}$.

Fig. 17 compares the coherent receiver architecture with an architecture that processes just one pilot signal, for 1 non-coherent integration (100 ms shots). According to the probability of acquisition depicted in Fig. 19, which also considers a P_a of 0.9 and 1 non-coherent integration, the theoretical limits are, respectively, 24.25 dBHz for the coherent architecture and 27.25 dBHz for the single pilot architecture. It can also be seen that the estimator is able to deliver estimates around those values.

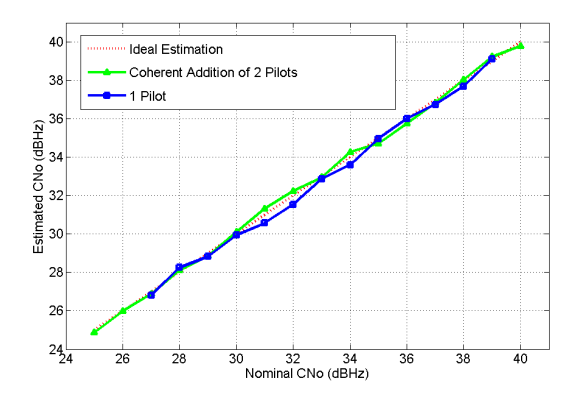


Figure 17 Performance of the CN_o estimators for the architecture that adds the pilots coherently and for one acquiring only 1 pilot. $N_c = 100$, $N_I = 1$, $P_{fa} = 10^{-8}$.

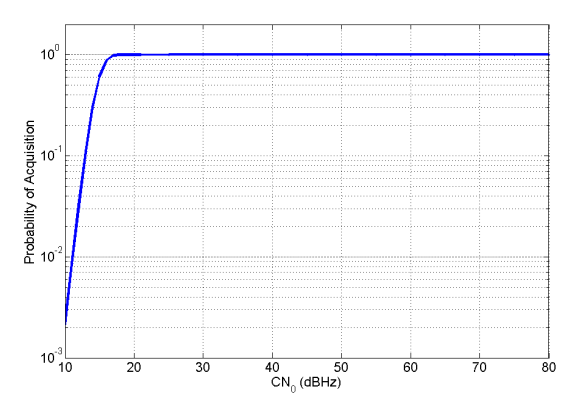


Figure 18 Probability of Acquisition vs CN_o. Galileo E5 coherent architecture. $N_c = 100$, $N_I = 10$, $P_{fa} = 10^{-8}$.

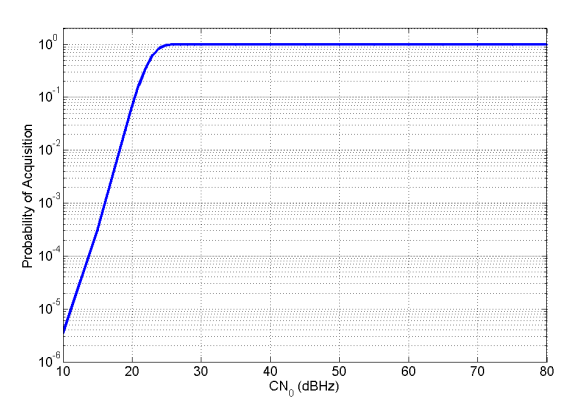


Figure 19 Probability of Acquisition vs CN_o. Galileo E5 coherent archtecture. $N_c = 100$, $N_I = 1$, $P_{fa} = 10^{-8}$.

The CN_o estimator can therefore deal with low signal levels encountered in weak signal scenarios.

PROCESSING TIMES TRENDS IN AND ACHIEVABLE SENSITIVITIES

The achievable sensitivity or detected CN_o is a function of the processing time. 35 dBHz, 30 dBHz or even 25 dBHz signals have been acquired with only 100 ms of data with this architecture. But to reach sensitivities below 25 dBHz, multiples of 100 ms are required. For instance, and recalling Fig. 2, 200 ms are able to detect 20 dBHz signals.

But to really exploit the potential of the acquisition techniques implemented and to try to reach low sensitivities for reasonable shot durations, e.g. 1 (16.1 dBHz) or 2 seconds (13.95 dBHz), then at least 1000 ms and 2000 ms of data, respectively, are required.

COMPUTATIONAL COST AND PROCESSING POWER CONSIDERATIONS

A discussion on the computational complexity of the receiver architecture is noteworthy. To begin with, let us consider that each FFT and IFFT operation performs $N \cdot \log(2N)$ complex multiplications and $2N \cdot \log(2N)$ complex additions, where N is the number of samples. According to this, the number of operations as a function of the coarse delay bins, τ_{co} , coarse Doppler cells, f_{co} and non-coherent integrations N_I can be written as

$$NumOps = N_I \begin{cases} f_{co} \cdot [1194 \cdot L_c + 398 \cdot (A+B) + \\ + \tau_{co} \cdot [400 \cdot L_c + 2 \cdot L_c (C+D)]] \end{cases}$$
 (10)

where

$$A = 2 \cdot L_c \cdot \log(4 \cdot L_c); \qquad B = 2 \cdot A \tag{11}$$

$$A = 2 \cdot L_c \cdot \log(4 \cdot L_c); \qquad B = 2 \cdot A$$

$$C = 2 \cdot N_s \cdot \log(4 \cdot N_s); \qquad D = 2 \cdot C$$
(11)

Due to the fact that large processing times are required to achieve high sensitivities, the algorithms can be very expensive in terms of memory and computational cost. In fact, detections using 1 second of data are quite expensive, especially considering the size of the acquisition matrix (search space). Tests with fast computers have been carried out and the processing time results in an average of less than 4 minutes for processing 100 ms of data, using an Intel Xeon CPU @ 3.2 GHz with 4 processor cores and 16 GB of RAM. In this case, the large FFT matrix computations are computed in a few seconds. The major limitation arises from the slower transfer rate from and to the hard disk.

Due to the large number of operations and the large bandwidth required for the Galileo E5 receiver architecture, current DSP technologies are the best option to enable the use of our acquisition functions at a very fast processing rate, due to their better digital signal processing throughput capabilities.

As a result, the computational demand of a Galileo E5 acquisition receiver system is still very high, and its use is more likely aimed for applications requiring a static scenario (indoor), according to the current state of technology, in spite of the fact that use is made here of techniques that increase efficiency.

Of course, there is much room for improvement in terms of computation time. For instance, further optimization methods would include changing from Matlab to compiled code on a microprocessor, including the FFT-based strategies, which would remarkably speed up the operations. Thus, with some optimizations, this software receiver could definitely be used for the aimed applications.

In fact, a specialized DSP could enable the feasibility of these acquisition techniques. An example of that is the PowerFFT, a DSP-ASIC being developed by Delft-based company Eonic. It is arguably the world's fastest and most powerful programmable FFT-centric floating-point DSP, able to perform on-the-fly data compression as well. PowerFFT is able to process 100 million complex samples per second in continuous mode. It enables many types of FFT functionalities, as well as convolutions and correlations.

Let us therefore consider a PowerFFT DSP, accommodating all of the FFT techniques proposed in this thesis.

Taking into consideration (10) for the number of operations in one processing branch, it is possible to obtain processing times for different cases, as it is shown in Table 1.

The simplest case considers a low Doppler uncertainty (1kHz) and a theoretical sensitivity threshold of 24 dBHz (1 non-coherent integration). It would take about 2.5 minutes to obtain a delay-Doppler estimate.

Table 1 Processing times for different receiver configurations using the PowerFFT DSP as reference.

configurations using the rowert range as reference.				
Non-Coherent	1	1	5	10
Integrations				
Coarse Doppler				
Cells (Doppler	2	10	20	20
Uncertainty) (KHz)	(1)	(5)	(10)	(10)
Number of	150e8	7e10	7e11	1.5e12
Operations				
Achievable CNo	24	24	19	16
(dBHz)				
Processing Time				
(hours)	0.04 h	0.2 h	2 h	4 h

On the other hand, a more severe scenario considering a large Doppler uncertainty (10 KHz) and a threshold of 16 dBHz (10 non-coherent integrations) shows that almost 4 hours are needed to obtain a result. This analysis is however quite conservative, as for instance no compression rates have been considered.

Keeping the coherent correlation length at 100 ms and performing just one non-coherent integration can still be advantageous (compared to GPS L1 C/A receivers) in terms of multipath resistance (as it has been seen before), near-far problem resistance, code ambiguity resolution, fewer losses due to bit transitions, etc.

As said, this study on computational cost has not been conservative as it must also be considered that Galileo will not be fully operational until a few years from now, therefore by the time the first commercial receivers become widely available, DSP technology will offer better processing figures.

However, the major bottleneck for the receiver will still be the data storage capabilities, as each 4D acquisition matrix will be several GBits in size or even tens of GBits, depending on the sample rate. Of course, data compression techniques will play an important role here, but the main idea is that the limitation will mostly come from memory storage rather than processing power, especially on the severe scenarios under consideration.

CONCLUSIONS

This paper supports the expectation that Galileo will deliver a better quality service than current GNSS services in low signal environments. The acquisition architecture described here enhances the GNSS service under these extreme conditions, overcoming the major issues that GNSS receivers face in weak signal environments.

The receiver is able to acquire weak signals by just using Galileo E5 pilot signals, without a priori information about the Galileo data bit stream. Coherent addition of the pilot signals at the late stages of the acquisition architecture increases the sensitivity of the receiver system and its resistance to interference from other Galileo E5 signals (e.g., due to near-far or multipath). This receiver architecture therefore achieves a theoretical increase in gain of circa 5 dB with respect to the Galileo E1OS-C band, and about 3 dB with respect to GPS L1 C/A.

Moreover, the architecture is able to extend the coherent correlation intervals up to the length of the Galileo E5 secondary codes, finding spreading code transitions in a blind way. Further sensitivity increases are also possible with the addition of non-coherent integrations and the use of assisted information.

It has also been discussed that current DSP technologies would enable receiver designers to implement the techniques presented in this thesis. With such hardware it would be feasible to obtain the expected performance results while maintaining a reasonable level of computational complexity.

For instance, the emphasis put on the FFT and other operations such as those seen in the interpolation and shift techniques has aimed at improving the efficiency of the design, as these operations can be performed by actual DSP hardware. In addition, having a design based only on an acquisition stage, not requiring any tracking, and being fully software-based, would simplify considerably the power consumption, size and cost of the system.

Regarding this, the architecture has been partly optimized for speed by careful use of FFT and inverse FFT block processing, yet there is room for even further optimization. A promising approach is to switch from Matlab to compiled code on a raw machine. Another way of increasing speed would be to use integer instead of double precision floating point arithmetics. Thus, if properly optimized, the techniques would become practical for the mentioned applications.

The trend in GNSS receiver developments goes towards the integration of software receivers with devices such as PDAs or cell phones. With regard to applications using handheld devices, it is important to note that the hardware of these devices is the driving factor that shall allow the integration of our Galileo acquisition architectures in future mass-market handheld systems. Such a step would confirm the feasibility of porting our receiver systems to this type of application as well.

In particular, the use of FFT has already shown compatibility with OFDM-based handheld devices, e.g., wireless devices and 3G cell phones.

Additionally, as experimental Galileo receivers are still in their first stages of matureness, it is not likely that Galileo commercial receivers will be integrated in handheld platforms in the short-term. However, by the time this integration with Galileo becomes a reality, future hardware will have certainly shown a noticeable increase in processing power and capacity.

The new Galileo E5 snapshot software receiver system has been tested using data from GNSS BitGrabber equipment in conjunction with simulated noise. The digitally generated noise has been used to simulate a lowering of the received CN_o. Signals with CN_o figures as weak as 13.95 dBHz have been successfully detected with just two seconds of dwell time in accordance with the theory. Weaker signals are detectable if that time is increased by adding more non-coherent integrations. In addition, it is interesting to study the use of longer coherent data intervals (multiples of the spreading sequence, i.e., multiples of 100 ms), to detect even weaker

signals. However, with current technology, the associated computational load is extremely high.

To conclude, some final concerns and clues for future work are briefly addressed. For example, during the development of this work, Rinex files for Galileo E5 were not available. So, analyzing Position-Velocity-Time (PVT) solutions using Rinex files of the actual Galileo constellation or from a Galileo constellation simulator would be interesting in the future.

Finally, the implementation can be optimized, for instance changing from Matlab to compiled code and using hardware that can handle FFT operations.

ACKNOWLEDGMENTS

The work of Sergio Carrasco-Martos was partially supported by the Delft University of Technology; and also by the ESA National Trainee Program funded by the Spanish Ministry of Science and Innovation.

REFERENCES

- [1] N. Blanco-Delgado, D. Jimenez-Baños, G. Lopez-Risueno, G. Seco-Granados, "Acquisition of Galileo L1C in Weak Signal Environment with Secondary Code Synchronization", in 1st CNES Workshop on Galileo Signals and Signal Processing, 2006.
- [2] R. Bryant. "Assisted GPS, Using Cellular Telephone Networks for GPS Anywhere", in GPS World, May 2005.
- [3] European Union, European Space Agency. "European GNSS (Galileo) Open Service. Signal In Space Interface Control Document (OS SIS ICD)". 2010.
- [4] G. López-Risueño, G. Seco-Granados. "Measurement and Processing of Indoor GPS Signals Using a One-Shot Software Receiver", in 2nd ESA Workshop on Satellite Navigation User Equipment Technologies (NAVITEC 2004), 2004.
- [5] J.B.Y. Tsui. "Fundamentals of Global Positioning System Receivers: a Software Approach", Wiley, 2nd edition, 2005.
- [6] A.V. Oppenheim, R.W. Schafer, J.R. Buck. "Discrete Time Signal Processing", Prentice Hall, 2nd edition.
- [7] G. López-Risueño, G. Seco-Granados. "CNo Estimation and Near-Far Mitigation for GNSS Indoor Receivers", in Proc. of IEEE Vehicular Technology Conference (VTC). Vol. 61, pp. 2624-2628. May, 2005.
- [8] G. Lachapelle, H. Kuusniemi, D.T.H. Dao, G. MacGougam, M.E. Cannon. "HSGPS Signal Analysis and Performance under Various Indoor Conditions", in Navigation: Journal of the Institute of Navigation, Vol. 51, No. 1, pp. 29-43, 2004.